

000
001
002054
055
056

Multi-channel Weighted Nuclear Norm Minimization for Real Color Image Denoising

057
058
059003
004
005
006
007060
061
062
063

Anonymous ICCV submission

008
009
010
011064
065
066

Paper ID 572

012
013
014067
068
069

Abstract

015

070
071

The noise structures among the R, G, B channels of real images are quite different due to the preprocessing steps in digital camera pipelines. This makes the real image denoising problem much more complex than traditional grayscale image denoising. In this paper, we propose a multi-channel optimization model for real color image denoising. Specifically, we introduce a weighting matrix into the data term to process adaptively each part of R, G, B channels in the joint patches concatenated by corresponding patches in these channels. In the regularization term, we employ the weighted nuclear norm to exploit the non-local self similar property. The proposed multi-channel weighted nuclear norm minimization (MC-WNNM) model is much more complex than the standard WNNM model. To solve this new problem, we reformulate the MC-WNNM model into a linear equality-constrained problem and solve it under the alternating direction method of multipliers (ADMM) framework. Each alternative updating step has closed-form solution and the convergence results are given. Experiments on benchmark datasets demonstrate that the proposed model outperforms state-of-the-art denoising methods on synthetic as well as real-world noisy images.

038
039080
081

1. Introduction

040
041082
083

Image denoising is an important problem in enhancing the image quality in computer vision systems. The traditional grayscale image denoising problem aims to recover the clean image \mathbf{x} from the noisy observation $\mathbf{y} = \mathbf{x} + \mathbf{n}$, where \mathbf{n} is often assumed to be additive white Gaussian noise (AWGN). Most image denoising methods in this field either employ the non-local self similarity (NSS) of natural images [1–7] or learn generative or discriminative denoisers from paired natural clean images and synthetic noisy images [8–12]. Among these methods, the weighted nuclear norm minimization (WNNM) method achieves excellent denoising performance by exploiting the NSS property

via low rank regularization.

The real color image denoising problem is not a trivial extension from single channel (grayscale image) to multiple channels (color image). The reason is that the noise in standard RGB (sRGB) space, though could be modeled as AWGN, are with different variances for different channels [13] due to the on-board processing steps in digital camera pipelines [14, 15]. This makes the real color image denoising problem much more complex. Directly applying the denoising methods for grayscale images to each channel of color images separately would obtain bad performance [16]. There are several work [14, 16–20] proposed specifically for color image denoising. The method [17] first transforms the color images into the luminance/chrominance space such as YCbCr before denoising, but this would make the noise distribution more complex in color images. The methods of [16, 20] process the joint patches concatenated by the corresponding patches in R, G, B channels and treat equally the patches in different channels. This would generate false colors or artifacts [16]. The methods of [14, 18, 19] ignore the non-local self similarity property of natural images, and their performance would be largely depressed [2, 7].

In order to deal with the R, G, B channels in color images more effectively, different noise properties of different channels should be considered in solving real color image denoising problem. Besides, due to its expressive denoising performance, the WNNM model [7] is employed to exploit the NSS property of natural images. In this paper, we proposed a multi-channel WNNM (MC-WNNM) model for real color image denoising. By introducing a weighting matrix to the WNNM model, the proposed MC-WNNM model no longer has closed-form solutions and more challenging to solve. By reformulating the proposed MC-WNNM model into a linear equality-constrained program with two variables, the relaxed problem can be solved under the alternating direction method of multipliers (ADMM) [21] framework. Each variable can be updated with closed-form solution [7, 22]. We also give the convergence results with detailed proof to guarantee a rational termination of the proposed algorithm.

108

2. Related Work

109

2.1. Weighted Nuclear Norm Minimization

111

As an extension to the nuclear norm minimization (NNM) model [23], the weighted nuclear norm minimization (WNNM) model [7] is described as

115

$$\min_{\mathbf{X}} \|\mathbf{Y} - \mathbf{X}\|_F^2 + \|\mathbf{X}\|_{\mathbf{w},*} \quad (1)$$

116

where $\|\mathbf{X}\|_{\mathbf{w},*} = \sum_i w_i \sigma_i(\mathbf{X})$ is the weighted nuclear norm of matrix \mathbf{X} , and $\mathbf{w} = [w_1, \dots, w_n]^\top, w_i \geq 0$ is the weight vector, $\sigma_i(\mathbf{X})$ is the i -th singular value of matrix \mathbf{X} . According to the Corollary 1 of [24], the problem (1) has closed-form solution if the weights are non-decreasing

122

$$\hat{\mathbf{X}} = \mathbf{U} \mathcal{S}_{\mathbf{w}/2}(\Sigma) \mathbf{V}^\top \quad (2)$$

123

where $\mathbf{Y} = \mathbf{U} \Sigma \mathbf{V}^\top$ is the singular value decomposition [25] of \mathbf{Y} and $\mathcal{S}_\tau(\bullet)$ is the generalized soft-thresholding operator with weight vector \mathbf{w} :

124

$$\mathcal{S}_{\mathbf{w}/2}(\Sigma_{ii}) = \max(\Sigma_{ii} - w_{ii}/2, 0) \quad (3)$$

125

Though having achieved excellent performance on grayscale image denoising, the WNNM model would generate false colors or artifacts [16], if being directly extended to real color image denoising by processing each channel separately or joint vectors concatenated by multiple channels. In this paper, for real noisy image denoising, we propose a multi-channel WNNM model which preserve the power of WNNM and be able to process the differences among different channels.

126

2.2. Real Color Image Denoising

127

During the last decade, several denoising methods are proposed for real color image denoising [17–20]. Among them, the CBM3D [17] first transform the RGB image into luminance-chrominance space (e.g., YCbCr) and then apply the famous BM3D method [2] on each channel separately with the patches being grouped only in the luminance channel. In [18], the authors proposed the “Noise Level Function” to estimate and remove the noise for each channel in natural images. However, the methods processing each channel separately would achieve inferior performance than processing jointly these channels [16]. The methods of [19, 20, 26] perform real color image denoising by concatenating the patches in R, G, B channels into joint vectors. However, the concatenation would treat each channel equally and ignore the different noise properties among these channels. The method in [14] models the cross-channel noise in real noisy image as a multivariate Gaussian and the noise is removed by the Bayesian nonlocal means filter [27]. The commercial software Neat Image [28] estimates the noise parameters from a flat region of the given noisy image and filters the noise correspondingly. But

these methods [14, 28] ignore the non-local self similarity property of natural images [2, 7].

In this paper, we introduce a weighting matrix which add different weights to different channels for color image denoising. The proposed multi-channel method can effectively solve the problem of different noise structures among different channels.

3. Color Image Denoising via Multi-channel Weighted Nuclear Norm Minimization

3.1. The Problem

The color image denoising problem is to recover the clean image $\{\mathbf{x}_c\}$ from its noisy version $\mathbf{y}_c = \mathbf{x}_c + \mathbf{n}_c$, where $c \in \{r, g, b\}$ is the index of R, G, B channels and \mathbf{n}_c is the noise in c -th channel. According to [13], the noise in standard RGB (sRGB) space though could be modeled as additive white Gaussian (AWGN) with different variances for different channels. Therefore, it is problematic to directly apply denoising methods to the joint vectors concatenated by corresponding patches of the R, G, B channels. To validate this point, in Fig. 1, we show the clean image ‘‘kodim23’’ taken from the Kodak PhotoCD dataset, its degraded version generated by adding synthetic additive white Gaussian noise (AWGN) to each channel of ‘‘kodim23’’, and the denoised image by applying WNNM [7] on the joint vectors concatenated from R, G, B channels of the degraded image. The standard derivations of AWGN added to the R, G, B channels are $\sigma_r = 40$, $\sigma_g = 20$, $\sigma_b = 30$, respectively. The input standard derivation of the noise for the concatenated WNNM method is set as the Root Mean Square (RMS) of those in each channel, i.e., $\sigma = \sqrt{(\sigma_r^2 + \sigma_g^2 + \sigma_b^2)/3} = 31.1$. From Fig. 1, one can see that the concatenated WNNM method treating each channel equally would remain some noise in the R and B channel, while over-smoothing the G channel of the degraded image. Hence, if the patches of different channels are treated adaptively in the concatenated vectors, the degraded color images would be recovered with better visual qualities.

In order to process each channel differently while still exploiting the joint structures of the color images, in this paper, we introduce a weighting matrix \mathbf{W} to the concatenated WNNM method. Assume the matrix \mathbf{Y} containing the noisy patches in R, G, B channels as $\mathbf{Y} = [\mathbf{Y}_r^\top \mathbf{Y}_g^\top \mathbf{Y}_b^\top]^\top$, the corresponding clean matrix $\mathbf{X} = [\mathbf{X}_r^\top \mathbf{X}_g^\top \mathbf{X}_b^\top]^\top$, and the weights \mathbf{w} for the singular values of \mathbf{X} , then the proposed multi-channel WNNM (MC-WNNM) model is

$$\min_{\mathbf{X}} \|\mathbf{W}(\mathbf{Y} - \mathbf{X})\|_F^2 + \|\mathbf{X}\|_{\mathbf{w},*}. \quad (4)$$

How to set the weighting matrix \mathbf{W} and how to solve the proposed model will be introduced in the next sections.

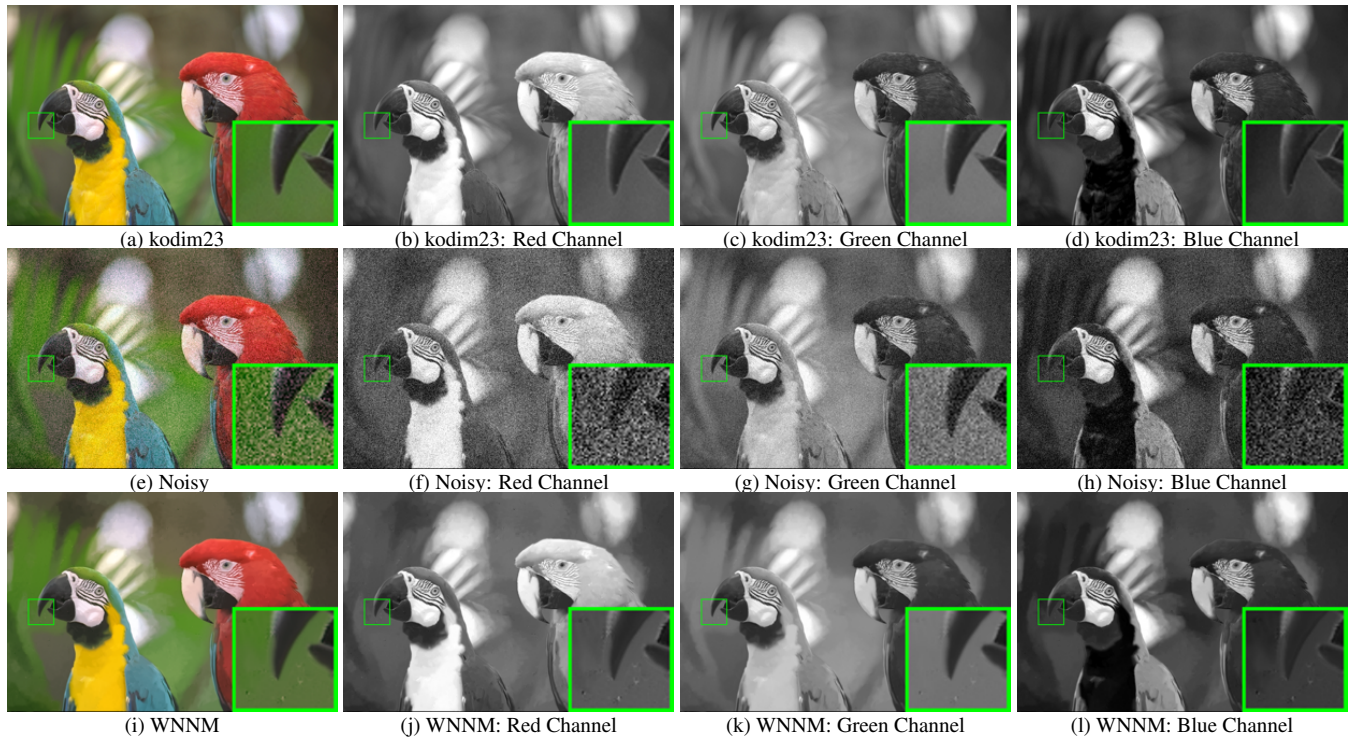


Figure 1. The image “kodim23” of the Kodak PhotoCD dataset, its degraded version, and the image recovered by WNNM. The R, G, B channels are also listed here for image quality comparison.

3.2. The Setting of Weighting Matrix \mathbf{W}

For simplicity, in this paper, we assume the noise are independent among the R, G, B channels and i.i.d. in each channel. Therefore, the weighting matrix \mathbf{W} is diagonal and can be determined under the Bayesian framework:

$$\begin{aligned} \hat{\mathbf{X}} &= \arg \max_{\mathbf{X}} \ln P(\mathbf{X}|\mathbf{Y}, \mathbf{w}) \\ &= \arg \max_{\mathbf{X}} \{\ln P(\mathbf{Y}|\mathbf{X}) + \ln P(\mathbf{X}|\mathbf{w})\}. \end{aligned} \quad (5)$$

The log-likelihood term $\ln P(\mathbf{Y}|\mathbf{X})$ is characterized by the statistics of noise, which is assumed to be channel-wise independent white Gaussian with standard deviations $\{\sigma_r, \sigma_g, \sigma_b\}$

$$P(\mathbf{Y}|\mathbf{X}) = \prod_{c \in \{r,g,b\}} (2\pi\sigma_c^2)^{-\frac{3p^2}{2}} \exp\left(-\frac{1}{2\sigma_c^2} \|\mathbf{Y}_c - \mathbf{X}_c\|_F^2\right). \quad (6)$$

We assume that the matrix \mathbf{X} follows the following distribution

$$P(\mathbf{X}|\mathbf{w}) \propto \exp\left(-\frac{1}{2} \|\mathbf{X}\|_{\mathbf{w},*}\right). \quad (7)$$

Putting (7) and (6) into (5), we have

$$\hat{\mathbf{X}} = \arg \min_{\mathbf{X}} \|\mathbf{W}(\mathbf{Y} - \mathbf{X})\|_F^2 + \|\mathbf{X}\|_{\mathbf{w},*}, \quad (8)$$

where

$$\mathbf{W} = \begin{pmatrix} \sigma_r^{-1} \mathbf{I} & \mathbf{0} & \mathbf{0} \\ \mathbf{0} & \sigma_g^{-1} \mathbf{I} & \mathbf{0} \\ \mathbf{0} & \mathbf{0} & \sigma_b^{-1} \mathbf{I} \end{pmatrix}. \quad (9)$$

where $\mathbf{I} \in \mathbb{R}^{p^2 \times p^2}$ is the identity matrix. Hence, the weighting matrix \mathbf{W} is determined to contribute equal weights for the pixel values in the same channel, while different weights for those in different channels. The experimental (which will be introduced later) results have already demonstrated that this form of weighting matrix have already generated the best denoising performance on synthetic and real noisy images in benchmark datasets.

3.3. The Denoising Algorithm

In this section, with the proposed MC-WNNM model, we propose a denoising algorithm for color images. In our algorithm, given a noisy image \mathbf{y} , each local patch is extracted from it with patch size $p \times p \times 3$ and stretched to a patch vector $\mathbf{y}_j \in \mathbb{R}^{3p^2}$ concatenated by corresponding patches in R, G, B, channels. Then we search the M most similar patches to \mathbf{y}_j (including \mathbf{y}_j itself) by Euclidean distance in a $W \times W$ local region around it. We stack the M similar patches column by column to form a noisy patch matrix $\mathbf{Y}_j = \mathbf{X}_j + \mathbf{N}_j \in \mathbb{R}^{3p^2 \times M}$, where \mathbf{X}_j and \mathbf{N}_j the corresponding clean and noise patch matrices. Then, we can apply the proposed MC-WNNM model to \mathbf{Y}_j to estimate \mathbf{X}_j for color image denoising:

$$\min_{\mathbf{X}_j} \|\mathbf{W}_j(\mathbf{Y}_j - \mathbf{X}_j)\|_F^2 + \|\mathbf{X}_j\|_{\mathbf{w},*}. \quad (10)$$

where \mathbf{W}_j is defined in Eq. (9). Just as [24] did, the weight vector \mathbf{w} is set $w_i^{k+1} = \frac{C}{|\sigma_i(\mathbf{X}_k)| + \epsilon}$ and $\epsilon > 0$ is a small

324
Algorithm 1: Color Image Denoising by MC-WNNM
325 **Input:** Noisy image \mathbf{y} , noise levels $\{\sigma_r, \sigma_g, \sigma_b\}$;
326 **Initialization:** $\hat{\mathbf{x}}^{(0)} = \mathbf{y}, \mathbf{y}^{(0)} = \mathbf{y}$;
327 **for** $k = 1 : K_1$ **do**
328 1. Set $\mathbf{y}^{(k)} = \hat{\mathbf{x}}^{(k-1)}$;
329 2. Extract local patches $\{\mathbf{y}_j\}_{j=1}^N$ from $\mathbf{y}^{(k)}$;
330 **for** each patch \mathbf{y}_j **do**
331 3. Search non-local similar patches \mathbf{Y}_j ;
332 4. Apply the MC-WNNM model (10) to \mathbf{Y}_j and
333 obtain the estimated \mathbf{X}_j ;
334 **end for**
335 5. Aggregate $\{\mathbf{X}_j\}_{j=1}^N$ to form the image $\hat{\mathbf{x}}^{(k)}$;
336 **end for**
337 **Output:** Denoised image $\hat{\mathbf{x}}^{K_1}$.

340 number to avoid zero numerator. Note that when $\sigma_r = \sigma_g =$
341 σ_b , the multi-channel WNNM model will be reduced to the
342 concatenated WNNM model as a special case.

343 The multi-channel WNNM is applied to the noisy patch
344 matrix \mathbf{Y}_j of each local patch \mathbf{y}_j in the noisy image \mathbf{y} . And
345 then all the patches are aggregated together to form the final
346 recovered image $\hat{\mathbf{y}}$. To obtain better denoising results,
347 we perform the above denoising procedure for several (K_1)
348 iterations. The proposed MC-WNNM denoising algorithm
349 for color images is summarized in Algorithm 1.

3.4. Optimization

352 The proposed MC-WNNM model could not be solved
353 in an analytical form while the original WNNM model
354 [24] could. In the WNNM model, when the weights on
355 singular values are non-descending, the weighted nuclear
356 norm proximal operator [24] can have global optimum with
357 closed-form solution. However, such property is not valid
358 for the multi-channel WNNM model. The reason is that the
359 weighting matrix \mathbf{W} is added to the rows of matrix \mathbf{X} instead
360 of its singular values. Besides, the elements in \mathbf{W} is
361 not in a non-descending order with respect to the singular
362 value of \mathbf{X} . This makes the proposed model more difficult
363 to solve when compared to the original WNNM model.

364 By introducing an augmented variable \mathbf{Z} , the MC-
365 WNNM model is reformulated as a linear equality-
366 constrained problem with two variables \mathbf{X} and \mathbf{Z} :

$$368 \min_{\mathbf{X}, \mathbf{Z}} \|\mathbf{W}(\mathbf{Y} - \mathbf{X})\|_F^2 + \|\mathbf{Z}\|_{w,*} \quad \text{s.t. } \mathbf{X} = \mathbf{Z}. \quad (11)$$

370 Since the objective function is separable across the two variables,
371 the problem (11) can be solved under alternating direction
372 method of multipliers (ADMM) framework. We can
373 derive its augmented Lagrangian function:
374

$$375 \mathcal{L}(\mathbf{X}, \mathbf{Z}, \mathbf{A}, \rho) = \|\mathbf{W}(\mathbf{Y} - \mathbf{X})\|_F^2 + \|\mathbf{Z}\|_{w,*} \\ 376 \quad + \langle \mathbf{A}, \mathbf{X} - \mathbf{Z} \rangle + \frac{\rho}{2} \|\mathbf{X} - \mathbf{Z}\|_F^2 \quad (12)$$

378 where \mathbf{A} is the augmented Lagrangian multiplier and $\rho > 0$
379 is the penalty parameter. We initialize the matrix variables
380 \mathbf{X}_0 , \mathbf{Z}_0 , and \mathbf{A}_0 to be zero matrix of suitable size. By tak-
381 ing derivative of the Lagrangian function \mathcal{L} with respect to
382 the variables \mathbf{X} and \mathbf{Z} and setting the derivative function to
383 be zero, we can alternatively update the ADMM algorithm
384 iteratively as follows:

385 (1) **Update \mathbf{X} while fixing \mathbf{Z} and \mathbf{A} :**

$$386 \mathbf{X}_{k+1} = \arg \min_{\mathbf{X}} \|\mathbf{W}(\mathbf{Y} - \mathbf{X})\|_F^2 + \frac{\rho_k}{2} \|\mathbf{X} - \mathbf{Z}_k + \rho_k^{-1} \mathbf{A}_k\|_F^2 \\ 387 \quad (13)$$

388 This is a standard least squares regression problem with
389 closed-form solution:

$$390 \mathbf{X}_{k+1} = (\mathbf{W}^\top \mathbf{W} + \frac{\rho_k}{2} \mathbf{I})^{-1} (\mathbf{W}^\top \mathbf{W} \mathbf{Y} + \frac{\rho_k}{2} \mathbf{Z}_k - \frac{1}{2} \mathbf{A}_k) \\ 391 \quad (14)$$

392 (2) **Update \mathbf{Z} while fixing \mathbf{X} and \mathbf{A} :**

$$393 \mathbf{Z}_{k+1} = \arg \min_{\mathbf{Z}} \frac{\rho_k}{2} \|\mathbf{Z} - (\mathbf{X}_{k+1} + \rho_k^{-1} \mathbf{A}_k)\|_F^2 + \|\mathbf{Z}\|_{w,*} \\ 394 \quad (15)$$

395 According to the Theorem 1 in [24], given the $\mathbf{X}_{k+1} +$
396 $\rho_k^{-1} \mathbf{A}_k = \mathbf{U}_k \Sigma_k \mathbf{V}_k^\top$ be the SVD of $\mathbf{X}_{k+1} + \rho_k^{-1} \mathbf{A}_k$,
397 where $\Sigma_k = \begin{pmatrix} \text{diag}(\sigma_1, \sigma_2, \dots, \sigma_n) \\ \mathbf{0} \end{pmatrix} \in \mathbb{R}^{m \times n}$, then the
398 global optimum of the above problem is $\hat{\mathbf{Z}} = \mathbf{U}_k \hat{\Sigma}_k \mathbf{V}_k^\top$,
399 where $\hat{\Sigma}_k = \begin{pmatrix} \text{diag}(\hat{\sigma}_1, \hat{\sigma}_2, \dots, \hat{\sigma}_n) \\ \mathbf{0} \end{pmatrix} \in \mathbb{R}^{m \times n}$ and
400 $(\hat{\sigma}_1, \hat{\sigma}_2, \dots, \hat{\sigma}_n)$ is the solution to the following convex opti-
401 mization problem:

$$402 \min_{\hat{\sigma}_1, \hat{\sigma}_2, \dots, \hat{\sigma}_n} \sum_{i=1}^n (\sigma_i - \hat{\sigma}_i)^2 + \frac{2w_i}{\rho_k} \hat{\sigma}_i \\ 403 \quad \text{s.t. } \hat{\sigma}_1 \geq \hat{\sigma}_2 \geq \dots \geq \hat{\sigma}_n \geq 0. \quad (16)$$

404 According to the Remark 1 in [24], the problem above has
405 closed-form solution

$$406 \hat{\sigma}_i = \begin{cases} 0 & \text{if } c_2 < 0 \\ \frac{c_1 + \sqrt{c_2}}{2} & \text{if } c_2 \geq 0 \end{cases} \quad (17)$$

407 where $c_1 = \sigma_i - \epsilon$, $c_2 = (\sigma_i - \epsilon)^2 - \frac{8C}{\rho_k}$ and C is set as
408 $\sqrt{2n}$ by experience in image denoising.

409 (3) **Update \mathbf{A} while fixing \mathbf{X} and \mathbf{Z} :**

$$410 \mathbf{A}_{k+1} = \mathbf{A}_k + \rho_k (\mathbf{X}_{k+1} - \mathbf{Z}_{k+1}) \quad (18)$$

411 (4) **Update ρ_k :** $\rho_{k+1} = \mu * \rho_k$, where $\mu > 1$.

412 The above alternative updating steps are repeated until
413 the convergence condition is satisfied or the number of
414 iterations exceeds a preset maximum number, e.g., K_2 .
415 The convergence condition of the ADMM algorithm is:
416 $\|\mathbf{X}_{k+1} - \mathbf{Z}_{k+1}\|_F \leq \text{Tol}$, $\|\mathbf{X}_{k+1} - \mathbf{X}_k\|_F \leq \text{Tol}$, and
417 $\|\mathbf{Z}_{k+1} - \mathbf{Z}_k\|_F \leq \text{Tol}$ are simultaneously satisfied, where
418 $\text{Tol} > 0$ is a small tolerance. We summarize the updating

Algorithm 2: Solve MC-WNNM via ADMM

Input: Matrices \mathbf{Y} and \mathbf{W} , $\mu > 1$, $\text{Tol} > 0$;

Initialization: $\mathbf{X}_0 = \mathbf{Z}_0 = \mathbf{A}_0 = \mathbf{0}$, $\rho_0 > 0$, $\mathbf{T} = \text{False}$, $k = 0$;

While ($\mathbf{T} == \text{false}$) **do**

1. Update \mathbf{X}_{k+1} as

$$\mathbf{X}_{k+1} = (\mathbf{W}^\top \mathbf{W} + \frac{\rho_k}{2} \mathbf{I})^{-1} (\mathbf{W}^\top \mathbf{W} \mathbf{Y} + \frac{\rho_k}{2} \mathbf{Z}_k - \frac{1}{2} \mathbf{A}_k)$$
2. Update \mathbf{Z}_{k+1} by solving the problem

$$\min_{\mathbf{Z}} \frac{\rho_k}{2} \|\mathbf{Z}\|_F^2 + \|\mathbf{Z}\|_{w,*}$$
3. Update \mathbf{A}_{k+1} as $\mathbf{A}_{k+1} = \mathbf{A}_k + \rho_k (\mathbf{X}_{k+1} - \mathbf{Z}_{k+1})$
4. Update $\rho_{k+1} = \mu * \rho_k$;
5. $k \leftarrow k + 1$;
if (Convergence conditions are satisfied) or ($k \geq K_2$)
5. $\mathbf{T} \leftarrow \text{True}$
end if

end while

Output: Matrices \mathbf{X} and \mathbf{Z} .

steps in Algorithm 2. The convergence analysis of the proposed Algorithm 2 is given in Theorem 1. Note that since the weighted nuclear norm is non-convex in general, we employ an unbounded sequence of $\{\rho_k\}$ here to make sure that the Algorithm 2 is convergent.

Theorem 1. Assume the weights in w are in a non-descending order, the sequence $\{\mathbf{X}_k\}$, $\{\mathbf{Z}_k\}$, and $\{\mathbf{A}_k\}$ generated in Algorithm 1 satisfy:

$$(a) \lim_{k \rightarrow \infty} \|\mathbf{X}_{k+1} - \mathbf{Z}_{k+1}\|_F = 0; \quad (19)$$

$$(b) \lim_{k \rightarrow \infty} \|\mathbf{X}_{k+1} - \mathbf{X}_k\|_F = 0; \quad (20)$$

$$(c) \lim_{k \rightarrow \infty} \|\mathbf{Z}_{k+1} - \mathbf{Z}_k\|_F = 0. \quad (21)$$

Proof. We give proof sketch here and detailed proof of this theorem can be found in supplementary files. We can first proof that the sequence $\{\mathbf{A}_k\}$ generated by Algorithm 3.4 is upper bounded. Since $\{\rho_k\}$ is unbounded, that is $\lim_{k \rightarrow \infty} \rho_k = +\infty$, we can proof that the sequence of Lagrangian function $\{\mathcal{L}(\mathbf{X}_{k+1}, \mathbf{Z}_{k+1}, \mathbf{A}_k, \rho_k)\}$ is also upper bounded. Hence, both $\{\mathbf{W}(\mathbf{Y} - \mathbf{X}_k)\}$ and $\{\mathbf{Z}_k\}$ are upper bounded. According to Eq. (18), we can proof that $\lim_{k \rightarrow \infty} \|\mathbf{X}_{k+1} - \mathbf{Z}_{k+1}\|_F = \lim_{k \rightarrow \infty} \rho_k^{-1} \|\mathbf{A}_{k+1} - \mathbf{A}_k\|_F = 0$, and (a) is proofed. Then we can proof that $\lim_{k \rightarrow \infty} \|\mathbf{X}_{k+1} - \mathbf{X}_k\|_F \leq \lim_{k \rightarrow \infty} \|(\mathbf{W}^\top \mathbf{W} + \frac{\rho_k}{2} \mathbf{I})^{-1} (\mathbf{W}^\top \mathbf{W} \mathbf{Y} - \mathbf{W}^\top \mathbf{W} \mathbf{Z}_k - \frac{1}{2} \mathbf{A}_k)\|_F + \rho_k^{-1} \|\mathbf{A}_k - \mathbf{A}_{k-1}\|_F = 0$ and hence (b) is proofed. Then (c) can be proofed by checking that $\lim_{k \rightarrow \infty} \|\mathbf{Z}_{k+1} - \mathbf{Z}_k\|_F \leq \lim_{k \rightarrow \infty} \|\Sigma_{k-1} - S_{w/\rho_{k-1}}(\Sigma_{k-1})\|_F + \|\mathbf{X}_{k+1} - \mathbf{X}_k\|_F + \rho_k^{-1} \|\mathbf{A}_{k-1} + \mathbf{A}_{k+1} - \mathbf{A}_k\|_F = 0$, where $\mathbf{U}_{k-1} \Sigma_{k-1} \mathbf{V}_{k-1}^\top$ is the SVD of the matrix $\mathbf{X}_k + \rho_{k-1} \mathbf{A}_{k-1}$. \square

4. Experiments

We evaluate the proposed MC-WNNM method on synthetic and real color image denoising. We compare the proposed method with other state-of-the-art denoising methods including CBM3D [17], MLP [10], WNNM [7], TNRD [12], “Noise Clinic” (NC) [19, 26], and the commercial software Neat Image (NI) [28].

4.1. Implementation Details

In synthetic experiments, the noise levels in R, G, B channels are assumed to be known as $\sigma_r, \sigma_g, \sigma_b$. In the real cases, the noise levels in R, G, B channels can be estimated via noise estimation methods [29, 30]. In this paper, we employ the method of [30] for its state-of-the-art performance. For the CBM3D method [17], the input noise levels are the Root Mean Square (RMS) as

$$\sigma = \sqrt{(\sigma_r^2 + \sigma_g^2 + \sigma_b^2)/3}. \quad (22)$$

For the methods of MLP [10] and TNRD [12], we retrain the models on grayscale images following their corresponding strategies at different noise levels from $\sigma = 5$ to $\sigma = 75$ with gap of 5. The denoising on color images is performed by processing separately each channel with the model trained at the same (or nearest) noise levels. NC [19, 26] is a blind image denoising method, so we just submit the noisy images (synthetic or real) to [26] and perform denoising using the default parameters. NI [28] is a commercial software suitable for real image denoising, while the code of CC [14] is not released (but its results on the 15 real noisy images in [14] are available by requesting the authors). Hence, we only compare with CC and NI in real image denoising experiments, and do not compare with them in synthetic experiments.

In order to take fully comparison with the original WNNM method [24], we extended the WNNM method [24] for color image denoising in three directions: 1) we apply the WNNM method [24] on each channel separately with corresponding noise levels $\sigma_r, \sigma_g, \sigma_b$. We call this method “WNNM0”; 2) we perform denoising on the joint vectors concatenated by corresponding patches in the R, G, B channels, where the input noise level σ is computed by RMS (Eq. (22)). We call this method “WNNM1”; 3) we set the weighting matrix \mathbf{W} in the proposed MC-WNNM model as $\mathbf{W} = \sigma^{-1} \mathbf{I}$. For fair comparison, we tune all these methods set the same parameters for “WNNM2” and the proposed MC-WNNM methods while achieving the best performance of “WNNM2”. For fair comparison, we tune the methods of “WNNM0”, “WNNM1”, “WNNM2”, and the proposed MC-WNNM to achieve corresponding best denoising performance (i.e., highest average PSNR results).

540

4.2. Experiments on Synthetic Noisy Images

In this section, we compare the proposed MC-WNNM method with other competing denoising methods [10, 12, 17, 19, 28] as well as the three extensions of the original WNNM method [24] on the 24 high quality color images from the Kodak PhotoCD Dataset (<http://r0k.us/graphics/kodak/>), which are shown in Fig. 2. The noisy images are generated by adding additive white Gaussian noise (AWGN) with known standard derivations $\sigma_r, \sigma_g, \sigma_b$ for the R, G, B channels, respectively. In this paper, the noise levels we add to each channel of the 24 color images are $\sigma_r = 40, \sigma_g = 20, \sigma_b = 30$, respectively. More experiments can be found in the supplementary files. For the methods of “WNNM2” and MC-WNNM, we set the patch size as $p = 6$, the number of non-local similar patches as $M = 70$, the window size for searching similar patches as $W = 20$, the updating parameter $\mu = 1.001$, the number of iterations in Algorithm 1 as $K_1 = 8$, the number of iterations in Algorithm 2 as $K_2 = 10$. For “WNNM2”, the initial penalty parameter is set as $\rho_0 = 10$, while for the proposed MC-WNNM model, the penalty parameter is set as $\rho_0 = 3$.

The PSNR results are listed in Table 1 of the compared methods including CBM3D [17], MLP [10], TNRD [12], NI [28], NC [19, 26], “WNNM0” [24], “WNNM1”, “WNNM2” and the proposed MC-WNNM methods. The best PSNR results are highlighted in bold. One can see that on all the 24 images, our method achieves the highest PSNR values over the competing methods. On average PSNR, our proposed method achieves 0.48dB improvements over the “WNNM0” method and outperforms the “WNNM2” by 1.09dB. Fig. 3 shows a scene denoised by the compared methods. We can see that the methods of CBM3D and NC would remain some noise on the recovered images. The methods of MLP, TNRD, and “WNNM0”, which process separately the channels of color images, would over-smooth the images and generate false colors or artifacts. The method “WNNM1”, which process jointly the channels of color images, would not generate false colors, but still over-smooth the image. The “WNNM2”, which is the WNNM model solved by ADMM algorithm, would remain some noise on the image. By employing the proposed MC-WNNM model, our method preserves the structures (e.g., textures in windows and grass) better across the R, G, B channels and generate less artifacts than other denoising methods, leading to visually pleasant outputs. More visual comparisons can be found in the supplementary files.

4.3. Experiments on Real Noisy Images

In this section, we compare the proposed MC-WNNM method with other competing methods on the 15 real noisy images (Fig. 4). We do not compare with the “WNNM0” method due to limited space and its inferior performance.



Figure 2. The 24 high quality color images from the Kodak PhotoCD Dataset.

The noisy images were collected under controlled indoor environment. Each scene was shot 500 times under the same camera and camera setting. The mean image of the 500 shots is roughly taken as the “ground truth”, with which the PSNR can be computed. Since the image size is very large (about 7000×5000) and the 11 scenes share repetitive contents, the authors of [14] cropped 15 smaller images (of size 512×512) to perform experiments. For each real noisy image, the noise levels in R, G, B channels are estimated by [30]. Since the noise levels are small in real noisy images, for the method of MLP [10] and TNRD [12], we apply the trained models of corresponding methods and choose the best denoising results (highest average PSNR values). Both methods achieve best results when setting the noise levels of the trained models from $\sigma = 10$.

We perform quantitative comparison on the 15 cropped images used in [14]. The PSNR results are listed in Table 2 of the compared methods including CBM3D [17], MLP [10], TNRD [12], NC [19, 26], NI [28], CC [14] (copied from [14]), “WNNM1”, “WNNM2”, and the proposed MC-WNNM method. The highest PSNR results are highlighted in bold. On average PSNR, the proposed MC-WNNM method achieves 0.44dB improvements over the “WNNM1” method and outperforms the state-of-the-art denoising method CC [14] by 0.83dB. On 10 out of the whole 15 images, the proposed MC-WNNM method achieves the highest PSNR values. Both CC and “WNNM1” achieves highest PSNR results on 2 of 15 images. It should be noted that in the CC method, a specific model is trained for each camera and camera setting, while our method uses the same model for all cases. Fig. 5 shows the denoised images of a scene captured by Canon 5D Mark 3 at ISO = 3200. We can see that CBM3D, NC, NI and CC would either remain noise or generate artifacts, while TNRD, “WNNM1”, and “WNNM2” over-smooth much the image. By using the proposed MC-WNNM model achieves better visual quality results than other methods. More visual comparisons can be found in the supplementary files.

648

649

650

651

652

653

654

655

656

657

658

659

660

661

662

663

664

665

666

667

668

669

670

671

672

673

674

675

676

677

678

679

680

681

682

683

684

685

686

687

688

689

690

691

692

693

694

695

696

697

698

699

700

701

702

703

704

705

706

707

708

709

710

711

712

713

714

715

716

717

718

719

720

721

722

723

724

725

726

727

728

729

730

731

732

733

734

735

736

737

738

739

740

741

742

743

744

745

746

747

748

749

750

751

752

753

754

648

649

650

651

652

653

654

655

656

657

658

659

660

661

662

663

664

665

666

667

668

669

670

671

672

673

674

675

676

677

678

679

680

681

682

683

684

685

686

687

688

689

690

691

692

693

694

695

696

697

698

699

700

701

Table 1. PSNR(dB) results of different denoising algorithms on 24 natural images.

Image#	$\sigma_r = 40, \sigma_g = 20, \sigma_b = 30$								
	CBM3D	MLP	TNRD	NI	NC	WNNM0	WNNM1	WNNM2	MC-WNNM
1	25.24	25.70	25.74	23.85	24.90	26.01	25.95	25.58	26.66
2	28.27	30.12	30.21	25.90	25.87	30.08	30.11	29.80	30.20
3	28.81	31.19	31.49	26.00	28.58	31.58	31.61	31.20	32.25
4	27.95	29.88	29.86	25.82	25.67	30.13	30.16	29.84	30.49
5	25.03	26.00	26.18	24.38	25.15	26.44	26.39	25.32	26.82
6	26.24	26.84	26.90	24.65	24.74	27.39	27.30	26.88	27.98
7	27.88	30.28	30.40	25.63	27.69	30.47	30.54	29.70	30.98
8	25.05	25.59	25.83	24.02	25.30	26.71	26.75	25.26	26.90
9	28.44	30.75	30.81	25.94	27.44	30.86	30.92	30.29	31.49
10	28.27	30.38	30.57	25.87	28.42	30.65	30.68	29.95	31.26
11	26.95	28.00	28.14	25.32	24.67	28.19	28.16	27.61	28.63
12	28.76	30.87	31.05	26.01	28.37	30.97	31.06	30.58	31.48
13	23.76	23.95	23.99	23.53	22.76	24.27	24.15	23.52	24.89
14	26.02	26.97	27.11	24.94	25.68	27.20	27.15	26.55	27.57
15	28.38	30.15	30.44	26.06	28.21	30.52	30.60	30.13	30.81
16	27.75	28.82	28.87	25.69	26.66	29.27	29.21	29.02	29.96
17	27.90	29.57	29.80	25.85	28.32	29.78	29.79	29.16	30.40
18	25.77	26.40	26.41	24.74	25.70	26.63	26.56	26.01	27.22
19	27.30	28.67	28.81	25.40	26.52	29.19	29.22	28.67	29.57
20	28.96	30.40	30.76	24.95	25.90	30.79	30.83	29.97	31.07
21	26.54	27.53	27.60	25.06	26.48	27.80	27.75	27.12	28.34
22	27.05	28.17	28.27	25.36	26.60	28.21	28.16	27.81	28.64
23	29.14	32.31	32.51	26.13	23.24	31.89	31.97	31.21	32.34
24	25.75	26.41	26.53	24.55	25.73	27.10	27.03	26.18	27.59
Average	27.13	28.54	28.68	25.24	26.19	28.84	28.83	28.22	29.31

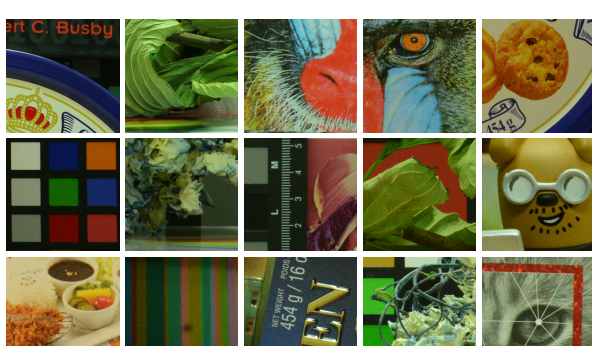
Figure 3. Denoised images of different methods on the image "kodim21" degraded by AWGN with different standard derivations of $\sigma_r = 40, \sigma_g = 20, \sigma_b = 30$ on R, G, B channels, respectively. The images are better to be zoomed in on screen.

Figure 4. The 15 cropped real noisy images used in [14].

5. Conclusion and Future Work

The real noisy images have different noise structures among the R, G, B channels due to the preprocessing steps

of the digital camera pipelines in CCD or CMOS sensors. This makes the real image denoising problem much more complex than grayscale image denoising. In this paper, we proposed a novel multi-channel (MC) model for real color image denoising. By introducing a weighting matrix to the concatenated weighted nuclear norm minimization (WNNM) model, the proposed MC-WNNM model can process adaptively the different noise structures in each of the R, G, B channels and exploit the non-local self similarity property of natural images. Though no longer having closed-form solution, we successfully solved the MC-WNNM model via an ADMM algorithm by reformulating the MC-WNNM model as a linear equality-constrained problem with two separable variables. We also studied the convergence property of the ADMM algorithm. Extensive experiments on synthetic and real color image denoising

Table 2. PSNR(dB) results of different methods on 15 cropped real noisy images used in [14].

Camera Settings	CBM3D	MLP	TNRD	NI	NC	CC	WNNM1	WNNM2	MC-WNNM
Canon 5D Mark III ISO = 3200	39.76 36.40 36.37	39.00 36.34 36.33	39.51 36.47 36.45	35.68 34.03 32.63	36.20 34.35 33.10	38.37 35.37 34.91	39.74 35.12 33.14	39.98 36.65 34.63	41.13 37.28 36.52
Nikon D600 ISO = 3200	34.18 35.07 37.13	34.70 36.20 39.33	34.79 36.37 39.49	31.78 35.16 39.98	32.28 35.34 40.51	34.98 35.95 41.15	35.08 36.42 40.78	35.08 36.84 39.24	35.53 37.02 39.56
Nikon D800 ISO = 1600	36.81 37.76 37.51	37.95 40.23 37.94	38.11 40.52 38.17	34.84 38.42 35.79	35.09 38.65 35.85	37.99 40.36 38.30	38.28 41.24 38.04	38.61 40.81 38.96	39.26 41.43 39.55
Nikon D800 ISO = 3200	35.05 34.07 34.42	37.55 35.91 38.15	37.69 35.90 38.21	38.36 35.53 40.05	38.56 35.76 40.59	39.01 36.75 39.06	39.93 37.32 41.52	37.97 37.30 38.68	38.91 37.41 39.39
Nikon D800 ISO = 6400	31.13 31.22 30.97	32.69 32.33 32.29	32.81 32.33 32.29	34.08 32.13 31.52	34.25 32.38 31.76	34.61 33.21 33.22	35.20 33.61 33.62	34.57 33.43 34.02	34.80 33.95 33.94
Average	35.19	36.46	36.61	35.33	35.65	36.88	37.27	37.12	37.71

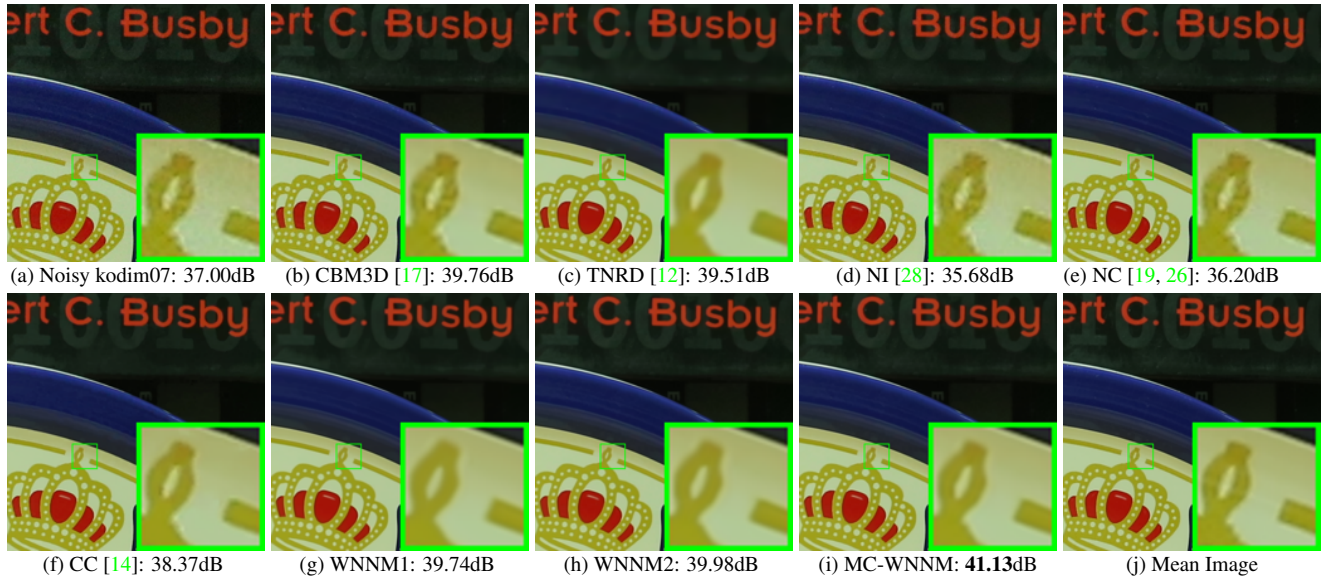


Figure 5. Denoised images of a region cropped from the real noisy image “Canon 5D Mark 3 ISO 3200 1” [14] by different methods. The images are better to be zoomed in on screen.

demonstrate that, the proposed MC-WNNM model outperforms the other competing denoising methods on both synthetic color noisy images as well as real-world noisy images. Introducing a weighting matrix can boost the performance of traditional models on new applications. We believe that this work can be extended in at least two directions. Firstly, the weighting matrix beyond the diagonal form, such as correlation form [31], may bring better performance on color image denoising. Secondly, the proposed MC-WNNM model can be further extended to deal with hyperspectral images, which may contain hundreds of

channels with different noise structures.

References

- [1] A. Buades, B. Coll, and J. M. Morel. A non-local algorithm for image denoising. *IEEE Conference on Computer Vision and Pattern Recognition (CVPR)*, pages 60–65, 2005. 1
- [2] K. Dabov, A. Foi, V. Katkovnik, and K. Egiazarian. Image denoising by sparse 3-D transform-domain collaborative filtering. *IEEE Transactions on Image Processing*, 16(8):2080–2095, 2007. 1, 2

- 864 [3] M. Elad and M. Aharon. Image denoising via sparse 918
865 and redundant representations over learned dictionaries. 919
866 *IEEE Transactions on Image Processing*, 15(12):3736–3745, 920
867 2006. 921
868
869 [4] J. Mairal, F. Bach, J. Ponce, G. Sapiro, and A. Zisserman. 922
870 Non-local sparse models for image restoration. *IEEE Interna- 923
871 tional Conference on Computer Vision (ICCV)*, pages 924
872 2272–2279, 2009. 925
873
874 [5] W. Dong, L. Zhang, G. Shi, and X. Li. Nonlocally central- 926
875 ized sparse representation for image restoration. *IEEE Transac- 927
876 tions on Image Processing*, 22(4):1620–1630, 2013. 928
877
878 [6] J. Xu, L. Zhang, W. Zuo, D. Zhang, and X. Feng. Patch 929
879 group based nonlocal self-similarity prior learning for image 930
880 denoising. *IEEE International Conference on Computer Vi- 931
881 sion (ICCV)*, pages 244–252, 2015. 932
882
883 [7] S. Gu, L. Zhang, W. Zuo, and X. Feng. Weighted nu- 933
884 clear norm minimization with application to image denoising. 934
885 *IEEE Conference on Computer Vision and Pattern Recog- 935
886 nition (CVPR)*, pages 2862–2869, 2014. 1, 2, 5
887
888 [8] S. Roth and M. J. Black. Fields of experts. *International 936
889 Journal of Computer Vision*, 82(2):205–229, 2009. 1
890
891 [9] D. Zoran and Y. Weiss. From learning models of natural 937
892 image patches to whole image restoration. *IEEE Interna- 938
893 tional Conference on Computer Vision (ICCV)*, pages 479– 939
894 486, 2011. 940
895
896 [10] H. C. Burger, C. J. Schuler, and S. Harmeling. Image 941
897 denoising: Can plain neural networks compete with BM3D? 942
898 *IEEE Conference on Computer Vision and Pattern Recog- 943
899 nition (CVPR)*, pages 2392–2399, 2012. 5, 6, 7
900
901 [11] U. Schmidt and S. Roth. Shrinkage fields for effective im- 944
902 age restoration. *IEEE Conference on Computer Vision and 945
903 Pattern Recognition (CVPR)*, pages 2774–2781, June 2014. 946
904
905 [12] Y. Chen, W. Yu, and T. Pock. On learning optimized re- 947
906 action diffusion processes for effective image restoration. 948
907 *IEEE Conference on Computer Vision and Pattern Recog- 949
908 nition (CVPR)*, pages 5261–5269, 2015. 1, 5, 6, 7, 8
909
910 [13] B. Leung, G. Jeon, and E. Dubois. Least-squares luma- 950
911 chroma demultiplexing algorithm for bayer demosaicking. 951
912 *IEEE Transactions on Image Processing*, 20(7):1885–1894, 952
913 2011. 1, 2
914
915 [14] S. Nam, Y. Hwang, Y. Matsushita, and S. J. Kim. A holistic 953
916 approach to cross-channel image noise modeling and its ap- 954
917 plication to image denoising. *IEEE Conference on Computer 955
918 Vision and Pattern Recognition (CVPR)*, pages 1683–1691, 956
919 2016. 1, 2, 5, 6, 7, 8
920
921 [15] H. C. Karaimer and M. S. Brown. A software platform for 957
922 manipulating the camera imaging pipeline. *European Con- 958
923 ference on Computer Vision (ECCV)*, October 2016. 1
924
925 [16] Julien Mairal, Michael Elad, and Guillermo Sapiro. Sparse 959
926 representation for color image restoration. *IEEE Transac- 960
927 tions on Image Processing*, 17(1):53–69, 2008. 1, 2
928
929 [17] K. Dabov, A. Foi, V. Katkovnik, and K. Egiazarian. Color 961
930 image denoising via sparse 3D collaborative filtering with 962
931 grouping constraint in luminance-chrominance space. *IEEE 963
932 International Conference on Image Processing (ICIP)*, pages 964
933 313–316, 2007. 1, 2, 5, 6, 7, 8
934
935 [18] C. Liu, R. Szeliski, S. Bing Kang, C. L. Zitnick, and W. T. 936
936 Freeman. Automatic estimation and removal of noise from 937
937 a single image. *IEEE Transactions on Pattern Analysis and 938
938 Machine Intelligence*, 30(2):299–314, 2008. 1, 2
939
940 [19] M. Lebrun, M. Colom, and J.-M. Morel. Multiscale image 941
941 blind denoising. *IEEE Transactions on Image Processing*, 942
942 24(10):3149–3161, 2015. 1, 2, 5, 6, 7, 8
943
944 [20] F. Zhu, G. Chen, and P.-A. Heng. From noise modeling to 945
945 blind image denoising. *IEEE Conference on Computer Vi- 946
946 sion and Pattern Recognition (CVPR)*, June 2016. 1, 2
947
948 [21] S. Boyd, N. Parikh, E. Chu, B. Peleato, and J. Eckstein. Dis- 949
949 tributed optimization and statistical learning via the alternat- 950
950 ing direction method of multipliers. *Found. Trends Mach. 951
951 Learn.*, 3(1):1–122, January 2011. 1
952
953 [22] C. Lu, C. Zhu, C. Xu, S. Yan, and Z. Lin. Generalized sin- 954
954 gular value thresholding. *AAAI*, 2015. 1
955
956 [23] J. Cai, E. J. Candès, and Z. Shen. A singular value thresh- 957
957 olding algorithm for matrix completion. *SIAM Journal on 958
958 Optimization*, 20(4):1956–1982, 2010. 2
959
960 [24] S. Gu, Q. Xie, D. Meng, W. Zuo, X. Feng, and L. Zhang. 961
961 Weighted nuclear norm minimization and its applications to 962
962 low level vision. *International Journal of Computer Vision*, 963
963 pages 1–26, 2016. 2, 3, 4, 5, 6
964
965 [25] C. Eckart and G. Young. The approximation of one matrix by 966
966 another of lower rank. *Psychometrika*, 1(3):211–218, 1936. 967
967 2
968
969 [26] M. Lebrun, M. Colom, and J. M. Morel. The noise clinic: 970
970 a blind image denoising algorithm. [http://www.ipol. 971
971 im/pub/art/2015/125/](http://www.ipol.im/pub/art/2015/125/). Accessed 01 28, 2015. 2, 5, 6, 7, 8
972
973 [27] C. Kervrann, J. Boulanger, and P. Coupé. Bayesian non- 974
974 local means filter, image redundancy and adaptive dictionar- 975
975 ries for noise removal. *International Conference on Scale 976
976 Space and Variational Methods in Computer Vision*, pages 977
977 520–532, 2007. 2
978
979 [28] Neatlab ABSoft. Neat Image. [https://ni. 979
980 neatvideo.com/home](https://ni.neatvideo.com/home). 2, 5, 6, 8
981
982 [29] X. Liu, M. Tanaka, and M. Okutomi. Single-image noise 983
983 level estimation for blind denoising. *IEEE Transactions on 984
984 Image Processing*, 22(12):5226–5237, 2013. 5

- 972 [30] G. Chen, F. Zhu, and A. H. Pheng. An efficient statistical 1026
973 method for image noise level estimation. *IEEE International 1027
974 Conference on Computer Vision (ICCV)*, December 2015. 5, 1028
975 6 1029
976 1030
977 [31] N. J. Higham. Computing the nearest correlation matrixa 1031
978 problem from finance. *IMA Journal of Numerical Analysis*, 1032
979 22(3):329, 2002. 8 1033
980 1034
981 1035
982 1036
983 1037
984 1038
985 1039
986 1040
987 1041
988 1042
989 1043
990 1044
991 1045
992 1046
993 1047
994 1048
995 1049
996 1050
997 1051
998 1052
999 1053
1000 1054
1001 1055
1002 1056
1003 1057
1004 1058
1005 1059
1006 1060
1007 1061
1008 1062
1009 1063
1010 1064
1011 1065
1012 1066
1013 1067
1014 1068
1015 1069
1016 1070
1017 1071
1018 1072
1019 1073
1020 1074
1021 1075
1022 1076
1023 1077
1024 1078
1025 1079